14. Sedimentology of Open-Ocean Biogenic Sediments from ODP Leg 201, Eastern Equatorial Pacific (Sites 1225 and 1226)[1]

Ivano W. Aiello[2] and Kathleen Kellett[2]

ABSTRACT

This paper reports methodology and results of sedimentologic analyses performed on biogenic sediments collected during Ocean Drilling Program Leg 201 in the eastern equatorial Pacific (Sites 1225 and 1226). Particle size analyses were carried out with a laser particle sizer on both bulk and noncarbonate fractions to document changes in the relative proportions of the main biogenic, biocalcareous, and biosiliceous components of these sediments. The grain size distribution of these very fine grained sediments is generally polymodal and characterized by main modes at ~10, ~17, and ~40 µm and minor modes at ~100 µm and ~1 mm. The modes represent the common biogenic components of these pelagic sediments, including coccoliths (~2–10 µm), pennate (~10–20 µm) and centric diatoms (~20–50 µm), radiolarian tests (~40–100 µm), juvenile foraminifers (~40–50 µm), fecal pellets (>50 µm), and test and frustule fragments (~10–100 µm). Downcore variations of particle sizes correlate with both small-scale and main lithologic changes in the sediment column and show pronounced shifts at unit/subunit boundaries at both eastern equatorial Pacific sites. Larger particle sizes characterize the units dominated by biosiliceous sediments. This relationship is particularly pronounced for the deeply buried diatom oozes (deeper than ~200 meters below seafloor) deposited during the late Miocene "carbonate crash." Conversely, the samples having the smallest grain sizes are concentrated in the coccolith oozes deposited during the late Miocene to Pliocene "biogenic bloom." Our

results also show that changes of some of the key dissolved chemicals involved in anaerobic microbial respiration and methanogenesis coincide with changes of sediment textures. In particular, the concentrations of the two main by-products of microbial respiration at these sites, reduced Fe and Mn, increase with the coarsening of the mean diameter and mode in the mixed diatom and radiolarian biosiliceous sediments of Pleistocene to Pliocene age and in the deeply buried late Miocene diatom oozes.

INTRODUCTION

The sedimentologic analyses presented in this paper were performed on sediment samples collected during Ocean Drilling Program (ODP) Leg 201 in the eastern equatorial Pacific, Sites 1225 and 1226 (D'Hondt, Jørgensen, Miller, et al., 2003) (Fig. F1). The main purpose of this cruise was to document the extent of subseafloor life and compare the rates of microbial activities in two contrasting depositional settings: the open-ocean pelagic sediments of the oligotrophic eastern equatorial Pacific basin and the hemipelagic ocean-margin deposits of the eutrophic Peru margin basin. The lowest microbial rates were found in the biogenic sediments of the eastern equatorial Pacific, which also contained some of the lowest cell concentrations ever observed in deep-sea sediments. However, all of the microbial processes observed in the ocean-margin sediments were also observed in the open-ocean sediments (D'Hondt, Jørgensen, Miller, et al., 2003). In particular, onboard and postcruise geochemical, microbiologic, and lithologic analyses indicated that the highest subseafloor rates of microbial activity in the eastern equatorial Pacific occur in deeply buried biosiliceous sediments of Pliocene and Miocene age (D'Hondt et al., 2004; Parkes et al., 2005). Leg 201 data document large-scale relationships between lithology (and, conversely, paleoceanography), distribution, and rates of microbial activities (D'Hondt, Jørgensen, Miller, et al., 2003). However, postcruise research suggests that these relationships can also be verified at smaller lithologic boundaries, including subunit boundaries and meter-scale bedding alternations (D'Hondt et al., 2004; Parkes et al., 2005). The dominant electron-accepting pathways of the open-ocean eastern equatorial Pacific sediments are sulfate, manganese, and iron reduction. The comparison between interstitial water dissolved inorganic carbon (DIC) and ammonium profiles from the two sites also indicates that mineralization of organic material at the relatively organic carbon (OC) rich Site 1226 is several-fold higher than at Site 1225. The concentrations of methane, ammonium, DIC, and alkalinity peak in the middle of the sediment columns, whereas sulfate concentrations are lowest in the middle and lower parts of the sediment column. Nitrate and oxygen are only present at the ocean and basement interfaces. In the lower portion of the sediment columns, the vertical sequence of successive reduction zones is reversed as a result of water flow through the underlying basaltic basement (D'Hondt, Jørgensen, Miller, et al., 2003).

Paleoceanographic Setting

Modern deposition at the eastern equatorial Pacific sites occurs beneath a region of relatively high productivity and enhanced accumulation of biogenic sediments (Chavez and Barber, 1987). Site 1225 is located near the present boundary between the South Equatorial Cur-

F1. Location map, p. 15.
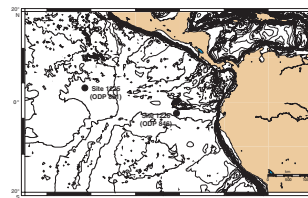
rent and the North Equatorial Countercurrent at 3670 m water depth. Site 1226 is located ~300 km south of the Galapagos Islands at 3297 m water depth beneath the present-day boundary between the South Equatorial Current and the nutrient-rich Peru Current (Fig. F1). Lithology, stratigraphy, and age model for Sites 1225 and 1226 (and nearby Sites 851 and 846) are described by Mayer et al. (1992), Pisias et al. (1995), and D'Hondt, Jørgensen, Miller, et al. (2003).

The biogenic sediments of Sites 1225 and 1226 consist mainly of Miocene to Pleistocene nannofossil (coccolith) ooze with varying amounts of biosiliceous (diatoms, radiolarians, and sponge spicules) and biocalcareous (foraminifers) microfossils and also accessory minerals (e.g., pyrite, plagioclase, dolomite, and hematite). The main mineralogic phases present in these sediments are calcite and silica (opal-CT and quartz) and reflect the composition of the two main biogenic components. Amorphous silica (opal-A) composes the frustules of living diatoms and is the major silica phase of the biosiliceous sedimentary component.

The stratigraphy of the eastern equatorial Pacific sites offers a continuous record of marine biogenic sedimentation from the early Miocene at Site 1226 (16.5 Ma) and the middle Miocene (11 Ma) at Site 1225 over cooling and subsiding basaltic crust (Mayer et al., 1992). Stratigraphic (vertical) changes of both lithology and physical properties account for the subdivision of the sedimentary column into units and subunits (D'Hondt, Jørgensen, Miller, et al., 2003). These lithologic changes reflect the evolution of biogenic sedimentation during the Neogene in the eastern equatorial Pacific, which earlier studies divided into three main paleoceanographic phases: the middle to late Miocene "carbonate crash," the late Miocene to early Pliocene "biogenic bloom," and late Pliocene to modern sedimentation (Pisias et al., 1995).

Grain Size Analyses of Pelagic Sediments

Particle size analyses, in conjunction with other sedimentologic and lithologic data, can improve the characterization of very fine grained biogenic sediments. Particle size variations can also be used to evaluate lithologic/textural controls and effects of microbial activity on biogenic sediments. Grain size analysis is a classic sedimentologic tool commonly used for the study of siliciclastic deposits, where particle sizes reflect the processes that generated the clasts, including weathering, erosion, transport, and sedimentation. There are relatively few examples of grain size studies of fine-grained biogenic sediments (e.g., Paull et al., 1988). However, in the last few years the number of detailed sedimentologic studies of pelagic and hemipelagic sediments has increased because analytical instruments that perform relatively rapid and automated analyses of very small particles have become available (McCave et al., 1995; Stuut et al., 2002; Warner and Domak, 2002). Grain size analyses of marine sediments have been successfully used in conjunction with other paleoceanographic proxies to document past changes in intensity of bottom currents and upwelling. For example, grain size analyses of carbonate oozes in sediment cores from the Walvis Ridge, southeast Atlantic Ocean, indicate that the last glacial episodes are marked by increasing fragmentation of foraminifer oozes (Stuut et al., 2002). Particle size analyses of Antarctic glacial marine sediments were successfully used by Warner and Domak (2002) as a paleoenvironmental proxy and correlated to downcore variations of magnetic susceptibility.

The analysis of fine-grained sediments has been commonly based on settling velocities and density differential between particles and a settling fluid (Stokes law, which applies only to perfectly spherical particles). However, most particles, including biogenic tests and test fragments, are not spherical, and the use of Stokes law yields grain sizes that tend to be finer than the actual particle sizes (Murray, 2002). Modern tools for particle size analysis are automated instruments that estimate grain size distribution based on different properties, including changes in intensity of a light beam that interacts with particles dispersed in a fluid (photohydrometer), X-ray attenuation (sedigraph), and electroresistance (Coulter counter). The laser particle sizer is a recently developed laser diffraction–based instrument that offers the most effective way to perform rapid analyses of very fine grained sediments on very small samples (<1 g). Particle size analyses were carried out with a Beckman-Coulter LS 13 320 laser particle size analyzer attached to an aqueous module equipped with a pump and a built-in ultrasound unit. The measured size distributions were analyzed from 0.04 μm to 2 mm. Measurements of such a wide particle size range are possible because the particle sizer is composed of two units: a laser beam for conventional (Fraunhofer) diffraction (from 0.4 μm to 2 mm) and a polarized intensity differential scatter (PIDS) unit, which measures particles based on the Mie theory of light scattering (0.04 μm; Beckman Coulter Inc., 2003).

The acquisition of biogenic sediment grain size data for samples from the eastern equatorial Pacific with a Beckman Coulter laser particle sizer first required the development of strategies for pretreatment and analysis of the samples. In particular, the "Materials and Methods" section, below, illustrates the experimental designs tested to establish disaggregation procedure and pretreatment of the indurated core sediment samples for grain size analysis with the particle sizer. The results of the tests and of the analyses are discussed in the following "Discussion," p. 7, section, and the grain size data are reported in the "Appendix," p. 13.

MATERIALS AND METHODS

Experimental procedures were designed to test the most reliable and consistent methods to study the particle size distributions and characterize the texture of Leg 201 samples with the combined use of a Beckman-Coulter LS 12 320 laser particle sizer and visual verification of compositions and sizes of the particles with optical petrography. The experiments were designed to address the problems involving the pretreatment methods necessary to disaggregate the sediments and their possible effects on sediment grains either by destroying or creating new particles. These problems include the effects of grinding of the dried and consolidated sample during subsampling and sample pretreatment and the effects of sonication on the sample in the liquid module of the particle sizer during the analysis. Verification of grain types, visual calibration of grain sizes, and identification of the effects of the pretreatment methods were carried out with petrographic microscopy analysis of smear slides. In order to characterize the relative contribution to the grain size distributions of the two main biosiliceous and biocalcareous sedimentary components, analyses were performed on both the bulk and noncarbonate fraction of the samples (the latter was obtained by reacting the sediment with HCl; see below).

Subsampling and Pretreatment

The biogenic calcareous and siliceous sediments of Leg 201 have a chalklike appearance because they have been drying for a few years since they were collected during Leg 201 in 2002. During subsampling, the core sediments break in irregular centimeter- to millimeter-size chunks that need to be disaggregated prior to particle size analysis. Subsampling was done by collecting a few grams of the indurated sediment and then grinding and powdering the subsample in a mortar with a ceramic pestle for a short time (~30 s; maximum = 1 min). The subsample was then separated in two aliquots (0.5 and 1.0 g) for analysis of bulk and noncarbonate fractions, respectively (see below). Given the very small size of the particles composing Leg 201 sediments (mean diameter is generally <60 µm) (Tables T1, T2), the bias introduced by grinding is probably negligible. However, the possible destructive effects of grinding on the pelagic particles were tested by analyzing the grain size distributions of the test samples over increasing amounts of grinding time (from 30 s to 5 min). The results of the tests supported our assumption that grinding of the samples for a short time (<1 min) does not alter the grain size distributions, which are significantly affected only by prolonged (>3 min) grinding.

Organic carbon is another component that can bind grains and forms particle aggregates that need to be dissolved with hydrogen peroxide before analysis. However, organic carbon in the eastern equatorial Pacific sediments is generally low (average = ~0.25 wt%) and rarely exceeds 1 wt% (D'Hondt, Jørgensen, Miller, et al., 2003), so treatment with H_2O_2 to oxidize organic matter was not necessary. Other factors however, may potentially affect the results of grain size analyses, including the destruction of clay minerals by HCl treatment (Stuut, 2002), corrosion of coccoliths by deionized water (Andruleit, 2000), and air bubbles in the liquid solution of the particle sizer.

After grinding, further disaggregation of the samples was first achieved by stirring the diluted sediment sample in a flask for a few seconds. Then, during particle size analysis, disaggregation was caused by the energy of the pump in the sample cell and, finally, by sonication. In order to establish the most reliable procedure for disaggregating the sediment while in the liquid module of the laser particle sizer and obtain reproducible particle size results that match visual observation on smear slide, several sonication tests were performed. Sonication is the most effective tool for the destruction of particle aggregates but can also add error to the measurements by creating new, smaller particles as a consequence of the fragmentation of whole fragile microfossil tests. For the biogenic sediments from the Walvis Ridge, Stuut et al. (2002) used 15 s of ultrasonic dispersion to prevent the fragmentation of delicate foraminifer tests. The optimal sonication time for carbonate-rich adhesive lake sediments was found to be 45 s (Murray, 2002).

The variations of mean diameter and mode with increasing sonication time for two test samples, diatom and nannofossil oozes (Samples 201-1226B-31X-3, 0 cm, and 24H-3, 0 cm, respectively) are shown in Figure F2A and F2C. The figure also shows the particle size distribution of the test samples at 0 s, 30 s, and 2 min sonication times (Fig. F2B, F2D). The results indicate that most of the decrease of the mean size occurs within the first few seconds of sonication, and after ~30 s the mean size decreases at a lower rate. However, the statistical results in Tables T1 and T2 show that on average there is ~50% reduction of mean size after 30 s of sonication in the bulk fraction and only a minor change in

T1. Grain size statistics, Site 1225, p. 24.

T2. Grain size statistics, Site 1226, p. 25.

F2. Sonication experiments, p. 16.
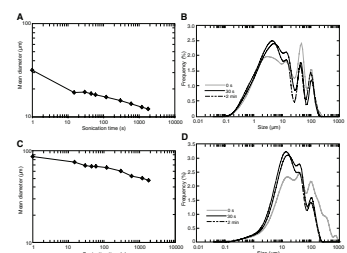
the noncarbonate fraction. Sonication is probably more effective in the bulk rather than in the noncarbonate fraction because of the strongly adhesive quality and highly charged molecules of carbonate-rich material (Murray, 2002). According to the results of the sonication experiments and the visual observations of the sediment samples under petrographic microscope, a sonication time of 30 s was chosen because it represents the best balance between the need to prevent the formation of aggregates in suspension and the need to prevent the formation of new particles due to the fragmentation of fragile biogenic debris.

Operating Conditions and Statistics

Subsampling of the solutions for the laser particle analysis was done with a pipette (diameter = >2 mm) while energetically stirring the flask to resuspend the sediment and ensure random sampling. Increasing amounts of the sediment solution were then added to the aqueous module of the particle sizer until obscuration values of 8%–12% and PIDS obscuration values of 48%–52% were obtained. Obscuration is the percentage or fraction of light that is attenuated because of extinction (scattering and/or absorption) by the particles and is also known as optical concentration.

The grain size analysis of the noncarbonate fraction was achieved by reacting the total carbon with HCl. Preparation of the noncarbonate fraction was done in conjunction with measurement of the weight percent total inorganic carbon (TIC). For TIC analyses, ~1 g of dry sediment was mixed with 10 mL of HCl in a sealed chamber, the pressure developed by the reaction was measured for 60 s, and the peak value was reported in pounds per square inch. Pressure values were converted to weight percent TIC by comparison with a standard curve. For more details on the gasometric method (carbonate "bomb"), see Schink et al. (1979). After reading the pressure, the lid of the chamber was removed and the remaining sample was resuspended in distilled water to increase the pH, in order to avoid formation and precipitation of reaction products. The sample was then rapidly moved to the sample cell of the aqueous module and measured for grain size.

Instrument settings during operations were as follows:

Pump speed = 70%.
Sonication power = 8.
Obscuration = 6–8.
Duration of each analysis = 90 s.

Deionized water was used to supply the liquid module. The optical model chosen for grain size determination is the default Fraunhofer model, based on the Fraunhofer theory of light scattering.

For all samples analyzed, grain size was also measured prior to sonication. The results of the analyses are reported in the "Appendix," p. 13, and the statistical summaries for Sites 1225 and 1226 are presented in Tables T1 and T2, respectively.

Data interpolation and statistical analyses were obtained with the laser particle sizer proprietary software (Beckman Coulter Inc., 2003). Because all samples analyzed tend to log-normal grain size distributions in the 0.04 µm to 2 mm spectrum, geometric rather than arithmetic statistics were applied to the values obtained by the logarithmically spaced size channels of the particle sizer. The statistical results of the grain size analyses of the samples from Sites 1225 and 1226 listed in the "Appen-

dix," p. 13, include the standard ODP sample header. Weight percent TIC determined with the gasometric method is also reported. Particle size data include the mean size and mode for both bulk and noncarbonate fractions for two sonication times (0 and 30 s). For the samples analyzed after 30 s of sonication, further statistical data listed include standard deviation (SD) and three percentiles (10%, 50%, and 90%).

DISCUSSION

The grain sizes of the sedimentary components of Leg 201 eastern equatorial Pacific sites (e.g., biogenic tests, frustules, coccoliths, skeletal parts, and fragments) occur within the range of sizes detectable with the laser particle sizer (0.04 μm to 2 mm).

At Site 1225, the shape of the average grain size distribution of the bulk fraction at 30 s of sonication is polymodal and characterized by a main mode at 9.87 μm, minor modes at 17.18, 39.77, and 101.1 μm, and a very small mode at 948.32 μm (Fig. F3A; Table T1). The modes represent the common particles that compose these pelagic sediments, including coccoliths (~2–10 μm), pennate (~10–20 μm) and centric (~20–50 μm) diatoms, radiolarian tests (~40–100 μm), juvenile foraminifers (~40–50 μm), fecal pellets (>50 μm), and fragments of microfossil tests and frustules (~10–100 μm). Similar relationships are observed in the frequency curves from the bulk fraction of samples from Site 1226 (Fig. F4), which show two distinct peaks at 13.61 and 43.66 μm, although the peak at ~110 μm is only minor. Mean, mode, and median are smaller in samples from Site 1225 (Table T1) than in samples from Site 1226 (Table T2). Larger average grain sizes in samples from Site 1226 may in part reflect the greater number of diatom oozes sampled in the core sediments retrieved in this site, as also shown by generally lower weight percent TIC (see the "Appendix," p. 13).

Total carbon data show that the noncarbonate fraction ranges between 10% and 80 wt% and is commonly <30% (see the "Appendix," p. 13). The particles of the noncarbonate fraction are the sedimentary components that survived dissolution by HCl and include biosiliceous tests such as diatom frustules, radiolarian tests, and other noncarbonate clasts. The frequency curves of the noncarbonate fraction at Sites 1225 and 1226 are very similar, characterized by a mode at ~15 μm that includes very small siliceous particles mostly composed of whole or dissolved/fragmented diatom frustules (Figs. F3B, F4B). The minor modes at 47.936 μm (43.667 μm) and 92.092 μm account for centric diatoms and radiolarian tests, respectively.

Downcore Variations of Particle Sizes

The particle size distributions of selected samples are shown in Figure F5, and examples of sediment microtextures are visualized by the smear slide microphotographs shown in Figure F6. Figures F7 and F8 show downcore variations of mean and mode of both the bulk and noncarbonate fractions after 30 s of sonication for Sites 1225 and 1226, respectively. In order to assess the relationships between sediment texture and lithology, the particle size data are plotted vs. depth and unit/subunit boundaries, luminosity (L*; generally carbonate-rich sediments have higher luminosity), and concentration of inorganic carbon (D'Hondt, Jørgensen, Miller, et al., 2003). The plot of Figure F8 shows that at Site 1226, downcore variations of sediment grain size mean and mode are
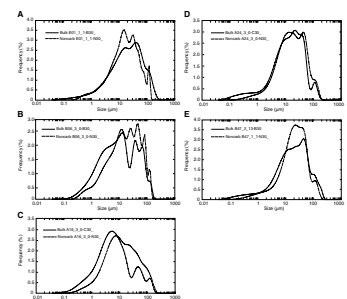
F3. Particle size frequency curve overlays, Site 1225, p. 17.
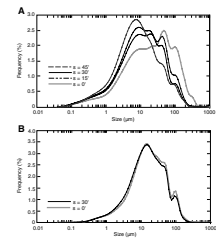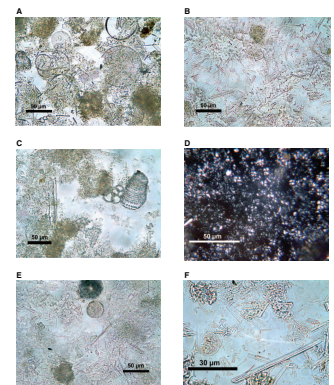

F4. Particle size frequency curve overlays, Site 1226, p. 18.
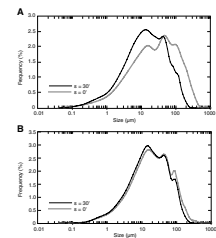
F5. Grain size distributions, p. 19.


F6. Microtextures, p. 20.

generally in opposition of phase with the variations of sediment luminosity and inorganic carbon. Conversely, the sediment samples with the coarsest grain sizes were detected in intervals characterized by lower luminosity, lower inorganic carbon, and the highest concentrations of biosilica (both diatoms and radiolarians).

The Pleistocene and late Pliocene shallow subseafloor sediments at both eastern equatorial Pacific sites are characterized by meter-scale alternations between nannofossil-rich diatom and radiolarian oozes and between diatom- and radiolarian-rich nannofossil oozes. This small-scale lithologic variability is reflected by the variability of both mean and mode between the samples collected in this interval, reflecting small-scale changes in the relative abundance of the siliceous and calcareous biogenic components (Figs. F5A, F5B, F7, F8) (see the "Appendix," p. 13). An overall bimodal, rightly skewed shape characterizes the particle size distributions of the samples from the uppermost Subunit IA at both Sites 1226 and 1225. In Sample 201-1226E-1H-1, 1 cm (Figs. F5A, F6A, F6B), the mode is centered at ~40 μm and corresponds to the occurrence of whole and fragmented centric diatoms, although fragments of radiolarian and foraminifer tests (~30–60 μm) are also included in the mode. A secondary mode at ~17 μm reflects the occurrence of large numbers of pennate diatoms. Microscopic observation shows the typically highly asymmetric elongated shape of pennate diatom frustules (Fig. F6B). The width of these siliceous microfossils ranges between ~2 and ~5 μm, and their elongation is highly variable, commonly ranging between ~5 and >100 μm, although values around 20 μm are common. The samples from the Pleistocene sediments are also characterized by a third minor mode at ~120 μm that describes the occurrence of relatively large fecal pellets and whole radiolarian tests. Calcite coccoliths are the smallest particles of these sediments (less than ~10 μm). In Figure F5B, the grain size distribution of a sample of mixed nannofossil, radiolarian, and diatom ooze collected in Subunit IA at Site 1226 near the Pliocene/Pleistocene boundary (Sample 201-1226B-6H-3, 0 cm) shows three modes centered at ~14 (pennate diatoms) and ~40 and ~70 μm (both centric diatoms) (Fig. F6C). The minor modes at ~70 and ~130 μm include larger siliceous microfossils such as whole and fragmented radiolarian tests, silicoflagellates, sponge spicules, and juvenile foraminifers, as well as calcite fragments from foraminifer tests. The broad hump of the frequency plot between ~2 and 7 μm (Fig. F5B) accounts for the occurrence of coccoliths generally more abundant in samples from the Pliocene sediments.

The coccolith oozes of the late Miocene to Pliocene "biogenic bloom" at both sites (Subunit IB at Site 1225 and Subunit IC at Site 1226) are characterized by very small grain sizes and generally show a single prominent mode and closer to log-normal particle size distribution (Figs. F5C, F6D). Downcore variations of both grain size mean and mode are only minimal and reflect the relatively homogeneous, calcareous lithology of the sediments from these stratigraphic intervals (Figs. F7, F8; see the "Appendix," p. 13). The frequency plot of Figure F5C (Sample 201-1225A-16H-3, 0 cm) shows the typical grain size distribution of a diatom-rich coccolith ooze from Site 1225 (Subunit IB), including a dominant mode at ~6 μm, with the most common size for coccoliths ranging between ~2 and ~10 μm (Fig. F6D). The hump between ~12 and 20 μm and the secondary mode at ~48 μm reflect the occurrence of pennate and centric diatoms, respectively. Fecal pellets and fragments of foraminifers account for the minor mode at ~140 μm (Fig. F5C).

F7. Mean diameter and mode, Site 1225, p. 22.
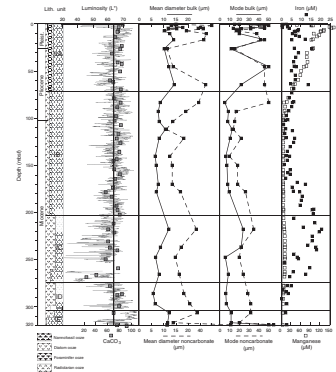
F8. Mean diameter and mode, Site 1226, p. 23.
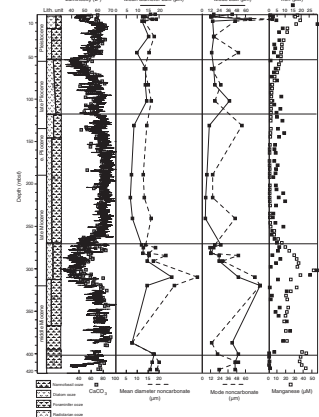
The coarser grain sizes of the deeply buried sediments deposited during the late Miocene "carbonate crash" reflect the abundance of the biosiliceous (mostly diatoms) microfossils over the calcareous coccoliths (Figs. F7, F8). The texture of the samples collected from these sediments are characterized by a polymodal grain size distribution similar to the texture of the biosiliceous Pliocene ooze (compare the frequency plots of Fig. F5A and F5D). In the frequency plot of Figure F5D (Sample 201-1225A-24H-3, 0 cm), the mode centered at ~23 μm accounts for the large amount of pennate diatoms (Fig. F6E, F6F). The occurrence of centric diatoms is reflected by the secondary mode at ~40 μm, whereas fecal pellets and whole and fragmented radiolarian tests account for a third minor mode at ~110 μm. Finally, the broad hump below ~10 μm, which also persists in the noncarbonate fraction, accounts for coccoliths and for fragmented/dissolved diatom frustules (Fig. F6G). These very small biosiliceous particles may be the result of fragmentation of diatom frustules by bottom currents winnowing the seafloor. Alternatively, the small size of the frustules can be the product of silica dissolution due to the opal-A to opal-CT silica phase change detected in these Miocene sediments by onboard mineralogic analyses (Shipboard Scientific Party, 2003).

At both Sites 1225 and 1226, the sediments directly overlying the basaltic oceanic crust have high concentrations of Fe and Mn oxides, which typically form reddish micronodules, mainly around radiolarian tests and fecal pellets (Figs. F5E, F6H, F6I). Sample 201-1226B-47X-2, 13 cm, from a radiolarian-rich nannofossil ooze shows that the oxides occur clustered in two main sizes: ~45 μm (mode) and ~110 μm (minor mode). Coccoliths in this sample are very abundant, and microscopic observations indicate that their size can be as large as ~12 μm, although they usually range between ~7 and ~9 μm (Figs. F5E, F6H, F6I).

In Figures F7 and F8, the downcore variations of sediment mean and mode are compared to pore water concentrations of the two main byproducts of subseafloor microbial activity in Leg 201 eastern equatorial Pacific Sites 1225 and 1226: reduced Fe and reduced Mn. These two chemical species show peak concentrations in the mixed, siliceous, and calcareous late Pliocene to Pleistocene sediments of Subunits IA at Site 1225 and IA and IB at Site 1226. As previously discussed, these relatively young and shallow subseafloor sediments are characterized by relatively coarse and variable grain sizes (e.g., the mean diameter ranges between ~10 and ~18 μm) (Figs. F7, F8; see the "Appendix," p. 13). At Site 1225, coarser grain sizes of the bulk and, in particular, noncarbonate fractions match peak concentrations of dissolved Mn at 3.6 meters below seafloor (mbsf) and a broad zone of relatively highly dissolved Fe centered at ~25 mbsf. Similar relationships are also verified for Site 1226, where dissolved Mn peaks just at the sediment/water interface and again at 9 mbsf. Pore water data also show active Mn reduction in the coarser biosiliceous oozes of the uppermost Subunit IA at both sites.

A correlation between coarsening of sediment texture and increased levels of microbial activity is also observed in the deeply buried late Miocene diatom oozes in Subunit IC at Site 1225 and, in particular, in Subunit ID at Site 1226. At the latter site, Mn reduction is the dominating electron-accepting pathway in the biosilica-rich opal-A and opal-CT sediments below 260 mbsf, with peaks at 300 mbsf and near the basement (Fig. F8). Conversely, at Site 1225 the dominant electron-accepting pathway is Fe reduction. Dissolved iron at this site shows a large peak centered at ~230 mbsf, which overlaps with minor Mn reduction,

as demonstrated by a broad zone of the dissolved element centered at ~250 mbsf.

CONCLUSIONS

This study demonstrates that standard petrographic microscopy in combination with high-resolution particle size analysis performed with a laser particle sizer equipped with a PIDS module (resolution 0.04 µm to 4 mm) is a powerful tool to detect and quantify compositional and textural changes of very fine grained pelagic sediments such as those of the eastern equatorial Pacific (ODP Leg 201, Sites 1225 and 1226). The small (<1 g) amount of sample required for the analysis makes this method particularly useful for describing small-scale lithologic and sedimentologic variations. The methodology that has been proposed for pretreatment and grain size analyses includes 30 s of sonication while the samples are sitting in the aqueous module of the laser particle sizer (Fig. F2). The method proposed also includes the separate grain size analysis of the bulk and noncarbonate fractions (the latter achieved by reacting the sediment with HCl; see the "Appendix," p. 13).

Our analyses indicate that in samples from Site 1225, the overall shape of the average grain size distribution of the bulk fraction at 30 s of sonication is polymodal and characterized by a main mode at 9.87 µm (Site 1226 = 13.61 µm), minor modes at 17.18, 39.77 (Site 1226 = 43.66 µm), and 101.1 µm (Site 1226 = 110 µm), and a very small mode at 948.32 µm (Figs. F3, F4; Tables T1, T2). The modes represent the common biogenic components of these pelagic sediments, including coccoliths (~2–10 µm), pennate (~10–20 µm) and centric (~20–50 µm) diatoms, radiolarian tests (~40–100 µm), juvenile foraminifers (~40–50 µm), fecal pellets (>50 µm), and test and frustule fragments (~10–100 µm).

At both sites, downcore variations of the textural characteristics of the sediments reflect lithologic variations and, consequently, variations in the proportions of coccoliths, pennate diatoms, centric diatoms, radiolarian and foraminifer fragments, fecal pellets, and trace amounts of silt-sized clasts and volcanic glass shards (Figs. F5, F6). Particle size statistics show that grain size changes correlate with main lithologic changes of the sediment column and show pronounced shifts at unit/subunit boundaries (Figs. F7, F8). At Site 1226, downcore variations of the mean diameter and mode are in opposition of phase with the coccolith-dominated oozes characterized by higher luminosity and inorganic carbon content. Conversely, they show a strong positive correlation with the darker, biosilica-rich sediments (both diatoms and radiolarians), showing the lowest concentrations of inorganic carbon. Our analyses indicate that the samples characterized by the smallest mean diameter and mode are concentrated in late Miocene to Pliocene coccolith-dominated calcareous sediments deposited during the "biogenic bloom." Conversely, coarser particle sizes were detected in the biosilica-rich radiolarian and diatom oozes of Pliocene and Pleistocene age and, in particular, in the deeply buried diatom oozes (deeper than ~200 mbsf) deposited during the late Miocene "carbonate crash."

Our results also show that at both Sites 1225 and 1226, downcore textural changes correlate with changes of some of the key dissolved chemicals involved in anaerobic microbial respiration and methanogenesis. Pore water concentrations of reduced Fe and reduced Mn are higher in the sediment of two stratigraphic intervals characterized by

high biosilica content and larger mean diameter and mode: the shallow subseafloor mixed, coccolith, radiolarian, and diatom oozes of Pleistocene to Pliocene age and the deeply buried late Miocene, opal-A, and opal-CT diatom oozes (Figs. F7, F8). This relationship is particularly pronounced in the late Miocene "carbonate crash" diatom oozes of Site 1226, which host unusually high levels of subseafloor microbial life, as indicated by an increased number of total and dividing cells (D'Hondt, Jørgensen, Miller, et al., 2003). In conclusion, our sedimentologic analyses suggest that in the sediments of the eastern equatorial Pacific, the depth distributions of modern microbial processes are related to the sediment's textural properties, which in turn were largely determined by past oceanographic conditions.

ACKNOWLEDGMENTS

REFERENCES

Andruleit, H.A., 2000. Dissolution-affected coccolithophore fluxes in the central Greenland Sea (1994/1995). *Deep-Sea Res., Part II,* 47:1719–1742. doi:10.1016/S0967-0645(00)00025-4

Beckman Coulter, Inc., 2003. *LS 13 320 Particle Size Analyzer Manual PN 7222061A:* Miami (Beckman).

Chavez, F.P., and Barber, R.T., 1987. An estimate of new production in the equatorial Pacific. *Deep-Sea Res. Part A,* 34:1229–1243. doi:10.1016/0198-0149(87)90073-2

D'Hondt, S.L., Jørgensen, B.B., Miller, D.J., et al., 2003. *Proc. ODP, Init. Repts.,* 201 [CD-ROM]. Available from: Ocean Drilling Program, Texas A&M University, College Station TX 77845-9547, USA. [HTML]

D'Hondt, S.L., Jørgensen, B.B., Miller, D.J., et al., 2004. Distributions of microbial activities in deep subseafloor sediments. *Science,* 306:2216–2221. doi:10.1126/science.1101155

McCave, I.N., Manighetti, B., and Robinson, S.G., 1995. Sortable silt and fine sediment size/composition slicing: parameters for palaeocurrent speed and palaeoceanography. *Paleoceanography,* 10:593–610. doi:10.1029/94PA03039

Mayer, L.A., Pisias, N.G., Janecek, T.R., et al., 1992. *Proc. ODP, Init. Repts.,* 138: College Station, TX (Ocean Drilling Program).

Murray, M.R., 2002. Is laser particle size determination possible for carbonate-rich lake sediments? *J. Paleolimnol.,* 27:173–183. doi:10.1023/A:1014281412035

Parkes, R.J., Webster, G., Cragg, B.A., Weightman, A.J., Newberry, C.J., Ferdelman, T.G., Kallmeyer, J., Jørgensen, B.B., Aiello, I.W., and Fry, J.C., 2005. Deep subseafloor prokaryotes stimulated at interfaces over geological time. *Nature (London, U. K.),* 436:390–394. doi:10.1038/nature03796

Paull, C.K., Hills, S.J., and Thierstein, H.R., 1988. Progressive dissolution of fine carbonate particles in pelagic sediments. *Mar. Geol.,* 81:27–40. doi:10.1016/0025-3227(88)90015-1

Pisias, N.G., Mayer, L.A., and Mix, A.C., 1995. Paleoceanography of the eastern equatorial Pacific during the Neogene: synthesis of Leg 138 drilling results. *In* Pisias, N.G., Mayer, L.A., Janecek, T.R., Palmer-Julson, A., and van Andel, T.H. (Eds.), *Proc. ODP, Sci. Results,* 138: College Station, TX (Ocean Drilling Program), 5–21.

Schink, C., Stockwell, J.H., and Ellis, R.A., 1979. An improved device for gasometric determination of carbonate in sediment. *J. Sediment. Res.,* 49:651–653.

Shipboard Scientific Party, 2003. Site 1225. *In* D'Hondt, S.L., Jørgensen, B.B., Miller, D.J., et al., *Proc. ODP, Init. Repts.,* 201, 1-86 [CD-ROM]. Available from: Ocean Drilling Program, Texas A&M University, College Station TX 77845-9547, USA. [HTML]

Stuut, J., Prins, M.A., and Jansen, J.H.F., 2002. Fast reconnaissance of carbonate dissolution based on the size distribution of calcareous ooze on Walvis Ridge, SE Atlantic Ocean. *Mar. Geol.,* 190:581–589. doi:10.1016/S0025-3227(02)00478-4

Warner, N.R., and Domack, E.W., 2002. Millennial- to decadal-scale paleoenvironmental change during the Holocene in the Palmer Deep, Antarctica as recorded by particle size analysis. *Paleoceanography,* 17. doi:10.1029/2000PA000602

APPENDIX

Table AT1. Results of particle size analyses. (Continued on next page.)

Core, section, interval (cm)	Depth (mbsf)	TIC (%)	Bulk mean diameter (0 s)	Standard deviation	Mode	Bulk mean diameter (30 s)	Standard deviation	Mode	Percentile		
									d10	d50	d90
201-											
1225C-1P-1, 37–47	0.37	75	29.08	4.738	55.13	14.84	5.776	19.76	2.348	21.35	112.8
1225A-1P-2, 0–15	1.5	51	52.98	5.051	168.9	13.01	4.386	45.75	1.83789	15.9321	69.0021
1225C-1P-3, 65	3.65	ND	35.94	3.892	66.44	17.91	3.867	45.75	2.74852	22.8795	74.4205
1225C-1P-4, 0–15	4.5	77	19.14	5.627	116.3	11.77	4.479	13.61	1.52895	13.4652	73.9354
1225C-1P-5, 0–15	6	ND	34.97	3.972	66.44	15.34	4.054	21.69	1.77164	19.6464	71.2106
1225A-2P-3, 0–15	7.3	82	29.11	4.897	55.13	10.23	4.641	19.76	1.36869	11.6584	65.0347
1225C-2P-1, 135–150	10.15	85	31.79	4.075	60.52	12.51	4.039	19.76	1.53138	16.2557	56.6561
1225A-3P-2, 135–150	16.65	73	41.4	4.972	153.8	14.06	4.362	45.75	2.04415	17.1912	75.169
1225A-4P-3, 0–15	26.3	ND	15.14	4.956	50.22	10.21	4.578	11.29	1.45856	10.596	73.4279
1225A-6P-3, 0–15	45.3	ND	25.08	5.125	127.6	12.14	4.477	50.22	1.78586	13.2517	74.3475
1225A-8P-3, 0–15	64.3	64	33.28	4.947	96.49	14.32	3.833	21.69	2.61892	16.3029	67.1497
1225A-10P-3, 0–15	83.3	ND	13.36	5.663	50.22	8.503	4.869	4.877	1.12954	8.4696	66.8442
1225A-11P-3, 0–15	92.8	78	13.84	4.624	37.97	7.752	4.271	8.536	1.16882	8.26747	51.1279
1225A-12P-3, 115–117	103.45	ND	8.555	4.756	5.878	8.12	4.265	7.775	0.895519	5.46011	32.3312
1225A-13P-3, 0–15	111.8	ND	16.99	4.539	45.75	10.7	4.097	12.4	1.67767	12.2913	54.8013
1225A-14P-3, 0–15	121.3	74	16.75	4.388	45.75	8.088	4.179	10.29	1.15323	9.216	44.8276
1225A-16P-3, 0–15	140.3	73	7.857	4.462	7.083	6.488	4.276	5.878	1.02132	6.17855	52.1754
1225A-18P-3, 0–15	159.3	ND	10.44	4.623	18	6.92	4.244	7.083	1.003	7.443	44.1
1225A-19P-3, 135–150	170.15	ND	17.07	5.15	55.13	7.761	4.151	7.775	1.21534	8.24899	45.8479
1225A-20P-3, 0–15	178.3	ND	8.405	3.525	8.536	6.959	3.538	9.37	1.23862	7.85709	31.5922
1225A-24P-3, 0–15	217.8	66	23.73	4.02	55.13	12.09	4.114	23.81	2.05098	14.8912	54.6793
1225A-26P-3, 0–15	236.8	63	13.02	4.256	41.68	8.646	3.895	21.69	1.51359	10.7808	38.0802
1225A-27P-3, 135–150	247.65	ND	7.066	4.068	5.878	6.625	4.036	5.354	1.18911	6.1814	48.2157
1225A-30P-2, 0–15	265.59	57	10.73	4.047	23.81	8.069	4.059	8.536	1.42238	8.8912	40.5125
1225A-32P-3, 0–15	286.07	81	10.39	4.883	37.97	5.625	4.271	5.878	0.757729	6.1455	32.7314
1225A-33P-3, 135–150	297.05	75	15.69	5.871	7.083	6.442	4.147	6.452	0.807198	7.45018	35.3236
1225A-34P-3, 0–15	306.7	86	25.46	4.472	50.22	12.21	4.516	11.29	1.73344	14.1866	62.4965
1225A-35P-3, 89–92	317.09	43	18.39	4.928	11.29	11.6	4.07	11.29	2.32	12.21	64.06
1225A-35P-5, 12–27	319.32	86	32.67	5.137	116.3	11.41	4.899	50.22	1.16933	13.6958	67.6716
1226E-1P-1, 15–21	0.15	62	31.35	4.944	127.6	18.18	4.059	41.68	2.84	21.5	96
1226E-1P-3, 15–21	3.15	21	16.39	3.501	18	13.32	3.228	13.61	2.99	14.1	55.6
1226E-1P-5, 0–6	6	21.1	16.08	4.883	87.9	16.84	4.708	66.44	2.03	18.7	112
1226B-2P-3, 85–91	8.25	41	18.67	3.961	41.68	12.19	3.847	14.94	2.12	13.4	64.4
1226B-4P-3, NA–NA	26.4	56.1	26.06	4.979	55.13	15.22`	4.363	16.4	2.06	17	97.4
1226B-6P-3, NA–NA	45.4	35	10.03	4.265	14.94	9.864	4.41	13.61	1.35	10.3	70.5
1226B-8P-3, 62–68	64.4	39	26.23	4.975	55.13	13.88	3.935	16.4	2.2	15.7	73.8
1226B-10P-3, NA–NA	83.4	22	13.28	3.631	16.4	13.72	3.72	18	2.44	14.9	71.1
1226B-12P-3, NA–NA	102.4	43.7	26.64	5	41.68	14.34	3.853	37.97	2.32	17	68.9
1226B-15P-3, 50–56	131.4	53.9	10.07	4.064	18	8.511	4.241	10.29	1.2	9.16	57.5
1226B-22P-4, NA–NA	189.4	ND	11.89	5.172	7.083	7.355	4.325	7.083	1.15	7	56.2
1226B-24P-3, NA–NA	216.4	73.8	8.605	4.989	50.22	6.842	4.543	5.354	0.946	6.5	54.4
1226B-27P-3, 57–63	240.97	70	11.01	5.094	41.68	7.801	4.612	4.877	1.12	7.37	62.2
1226E-15P-3, 20–26	272.2	38.4	20.75	4.732	19.76	11.98	3.54	26.14	2.25	12.9	57.5
1226B-30P-3, 55–61	275.45	62.4	43.41	5.626	127.6	12.8	4.503	11.29	1.81	14	85.9
1226B-16P-3, 55–61	282.05	49	23.24	4.644	14.94	12.58	3.9	12.4	2.32	13.7	67.6
1226B-31P-3, 19–20	284.69	9	31.62	4.462	45.75	15.39	3.184	23.81	3.43	16.6	61.1
1226E-17P-3, 20–26	291.2	29.9	25.76	4.351	41.68	14.56	3.305	23.81	3.07	16.6	56.6
1226E-19P-3, 20–26	310.2	19.3	69.99	4.149	153.8	25.8	3.647	50.22	4.66	33.9	103
1226E-20P-3, 66–72	320.16	55.7	25.1	5.142	87.9	14.51	4.652	80.07	2.05	16.4	90.7
1226E-22P-CC, 19–25	387.69	80	24.05	3.856	50.22	7.618	4.171	41.68	1.11	8.86	41.6
1226B-45P-3, 81–86	401.01	71	54.32	4.241	127.6	17.74	4.271	50.22	2.65	22.9	89.8
1226B-46P-3, 80–86	410.6	ND	45.95	4.675	153.8	16.83	3.999	45.75	2.95	20.1	84.5
1226B-47P-2, 139–145	419.29	67	32.66	4.549	80.07	15.95	4.369	45.75	2.48	19.6	84.6

Notes: ND = not determined, NA = not available. Percent TIC determined with the gasometric method.

Table AT1 (continued).

Core, section, interval (cm)	Depth (mbsf)	%TIC	Noncarbonate mean diameter (0 s)	Standard deviation	Mode	Noncarbonate mean diameter (30 s)	Standard deviation	Mode	Percentile		
									d10	d50	d90
201-											
1225C-1P-1, 37–47	0.37	75	19.14	3.037	19.76	15.3	3.004	14.94	3.08822	15.2982	63.0285
1225A-1P-2, 0–15	1.5	51	48.59	2.723	72.94	29.85	2.637	50.22	4.64798	18.2228	49.0238
1225C-1P-3, 65	3.65	ND	30.63	2.477	37.97	25.16	2.629	31.5	3.77426	18.0501	83.0467
1225C-1P-4, 0–15	4.5	77	33.52	3.108	50.22	24.12	2.975	45.75	3.72647	18.5166	63.3802
1225C-1P-5, 0–15	6	ND	36.2	2.422	45.75	26.26	2.517	31.5	2.89547	14.5076	61.9164
1225-2P-3, 0–15	7.3	82	20.75	2.831	31.5	19.35	3.075	16.4	3.05597	18.3154	89.0659
1225C-2P-1, 135–150	10.15	85	41.44	2.459	55.13	27.52	2.505	37.97	2.52825	12.0482	46.6402
1225A-3P-2, 135–150	16.65	73	39	2.64	55.13	26.55	2.591	41.68	4.7567	19.5903	57.2469
1225A-4P-3, 0–15	26.3	ND	16.07	4.054	41.68	11.37	4.026	14.94	ND	ND	ND
1225A-6P-3, 0–15	45.3	ND	34.82	3.322	60.52	13.82	3.404	45.75	ND	ND	ND
1225A-8P-3, 0–15	64.3	64	40.72	2.792	55.13	27.26	2.67	45.75	6.14229	24.3921	65.4142
1225A-10P-3, 0–15	83.3	ND	31.04	2.948	50.22	24.37	2.898	50.22	ND	ND	ND
1225A-11P-3, 0–15	92.8	78	25.5	2.934	50.22	19.13	3.205	16.4	2.70359	18.5466	87.8265
1225A-12P-3, 115–117	103.45	ND	18.26	3.256	28.7	13.72	3.252	14.94	ND	ND	ND
1225A-13P-3, 0–15	111.8	ND	13.92	3.872	34.58	11.09	3.969	13.61	ND	ND	ND
1225A-14P-3, 0–15	121.3	74	24.58	2.883	37.97	18.28	3.052	21.69	2.85929	14.8864	72.3006
1225A-16P-3, 0–15	140.3	73	14.04	3.559	11.29	12.56	3.62	9.37	2.20423	11.9811	74.082
1225A-18P-3, 0–15	159.3	ND	ND	ND	ND	13.49	3.686	18	ND	ND	ND
1225A-19P-3, 135–150	170.15	ND	21.41	3.486	41.68	13.49	3.686	18	ND	ND	ND
1225A-20P-3, 0–15	178.3	ND	22.21	3.118	41.68	16.89	3.08	26.14	ND	ND	ND
1225A-24P-3, 0–15	217.8	66	35.08	2.607	50.22	23.4	2.688	34.58	3.67664	17.8686	68.838
1225A-26P-3, 0–15	236.8	63	25.13	2.773	37.97	17.15	2.886	21.69	2.4705	12.1014	64.5714
1225A-27P-3, 135–150	247.65	ND	22.48	3.573	45.75	14.79	3.398	19.76	ND	ND	ND
1225A-30P-2, 0–15	265.59	57	20.78	2.711	31.5	16.4	2.87	23.81	2.55061	12.609	73.6366
1225A-32P-3, 0–15	286.07	81	22.65	2.92	28.7	18.33	3.05	28.7	2.73776	15.6576	72.0927
1225A-33P-3, 135–150	297.05	75	43.75	3.402	50.22	20.81	2.981	31.5	3.73317	16.3467	49.825
1225A-34P-3, 0–15	306.7	86	33.48	2.789	41.68	23.72	2.855	31.5	3.34563	16.9278	64.9543
1225A-35P-3, 89–92	317.09	43	17.44	3.905	11.29	13.82	3.247	19.76	3.125	14.48	57.97
1225A-35P-5, 12–27	319.32	86	57.92	2.402	96.49	37.6	2.379	55.13	3.7239	13.9782	34.1001
1226E-1P-1, 15–21	0.15	62	18.88	3.451	18	16.11	3.272	16.4	3.31825	17.6762	68.1398
1226E-1P-3, 15–21	3.15	21	13.6	3.349	12.4	12.49	3.274	12.4	2.72931	12.7641	59.0983
1226E-1P-5, 0–6	6	21.1	19.19	4.009	105.9	18.67	4.054	96.49	2.84502	19.971	104.967
1226B-2P-3, 85–91	8.25	41	13.52	3.817	87.9	13.16	3.974	45.75	2.19629	12.936	82.7524
1226B-4P-3, NA–NA	26.4	56.1	18.28	3.826	16.4	17.78	3.876	16.4	2.78529	18.9546	98.0276
1226B-6P-3, NA–NA	45.4	35	15.75	3.788	45.75	15.39	3.786	50.22	2.41268	17.446	80.443
1226B-8P-3, 62–68	64.4	39	14.36	3.752	14.94	13.25	3.675	13.61	2.30528	13.965	71.9617
1226B-10P-3, NA–NA	83.4	22	15.57	3.675	26.14	15.03	3.679	26.14	2.62875	16.7905	76.7716
1226B-12P-3, NA–NA	102.4	43.7	17.31	3.386	18	16.41	3.41	18	3.25962	18.1811	73.8178
1226B-15P-3, 50–56	131.4	53.9	14.96	3.577	18	14.38	3.594	55.13	2.44024	16.5516	66.062
1226B-22P-4, NA–NA	189.4	ND	14.74	4.281	16.4	12.75	4.182	14.94	1.89869	13.3073	81.1679
1226B-24P-3, NA–NA	216.4	73.8	13.44	3.979	16.4	13.23	4.021	14.94	2.03514	14.0774	78.5443
1226B-27P-3, 57–63	240.97	70	17.52	3.974	45.75	16.38	3.985	45.75	2.50863	17.7843	93.4558
1226E-15P-3, 20–26	272.2	38.4	16.02	3.716	18	13.85	3.427	18	2.72416	14.8888	65.2719
1226B-30P-3, 55–61	275.45	62.4	20.49	3.3	16.4	18.37	3.256	16.4	4.54885	19.0489	83.8082
1226E-16P-3, 55–61	282.05	49	16.11	3.221	12.4	15.35	3.2	12.4	3.48613	15.6564	71.5664
1226B-31P-3, 19–20	284.69	9	30.51	3.943	50.22	23.11	3.453	50.22	4.54178	26.9702	102.997
1226E-17P-3, 20–26	291.2	29.9	18.52	3.072	28.7	17.4	3.048	28.7	3.97	19.6898	62.8228
1226E-19P-3, 20–26	310.2	19.3	54.31	3.382	105.9	37.52	3.079	72.94	8.29614	50.0455	115.326
1226E-20P-3, 66–72	320.16	55.7	29.85	3.591	80.07	27	3.438	80.07	4.99915	33.8509	100.575
1226E-22P-CC, 19–25	387.69	80	17.84	3.873	96.49	7.667	2.789	13.61	2.10127	8.52254	23.1246
1226B-45P-3, 81–86	401.01	71	20.41	2.984	21.69	17.39	2.768	21.69	4.91827	19.4743	52.9058
1226B-46P-3, 80–86	410.6	ND	23.14	3.093	50.22	20.02	2.918	50.22	4.87465	22.725	66.554
1226B-47P-2, 139–145	419.29	67	23.63	3.606	23.81	18.99	3.198	23.81	4.31088	22.2098	66.8369

Figure F1. Location map, Sites 1225 and 1226. Previous ODP designations are in parentheses.
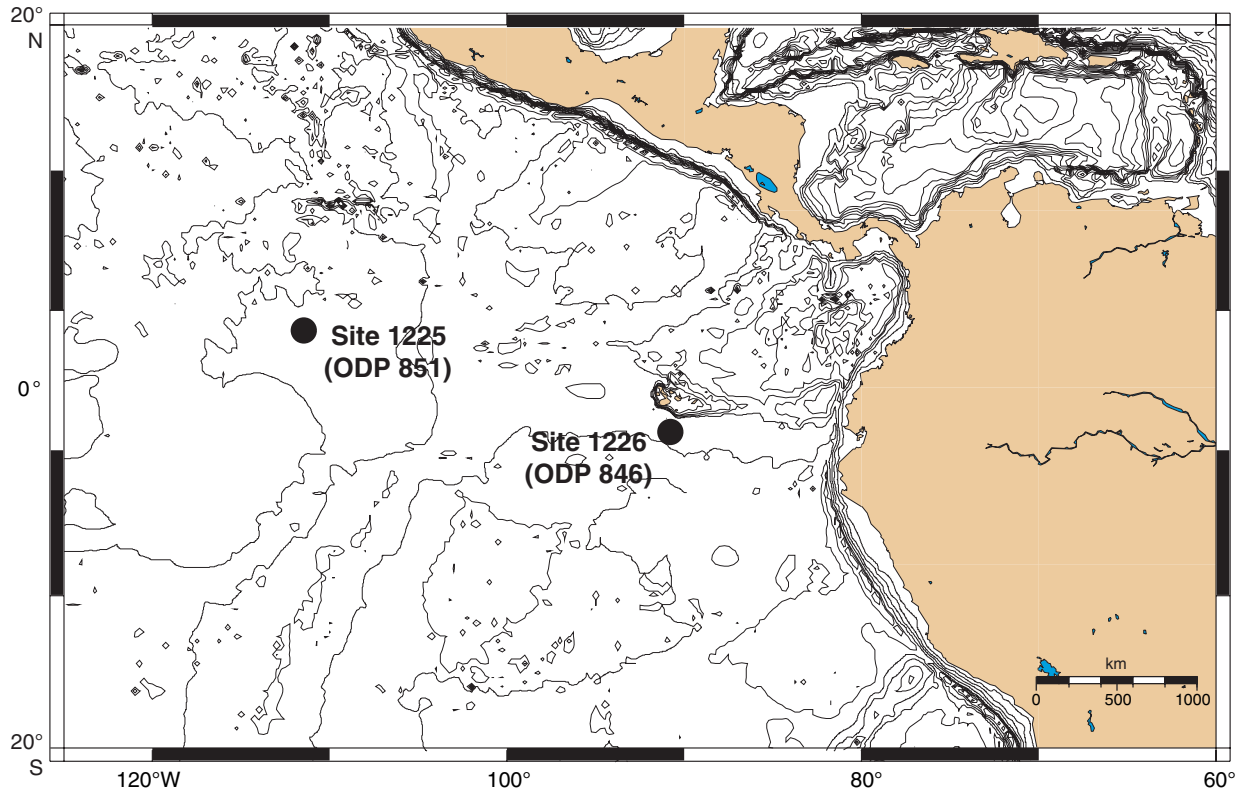
Figure F2. Results of sonication experiments for two contrasting lithologies of Leg 201 eastern equatorial Pacific sites. **A, B.** Diatom ooze (Sample 201-1226B-31X-3, 0 cm). **C, D.** Nannofossil ooze (Sample 201-1226B-24H-3, 0 cm).
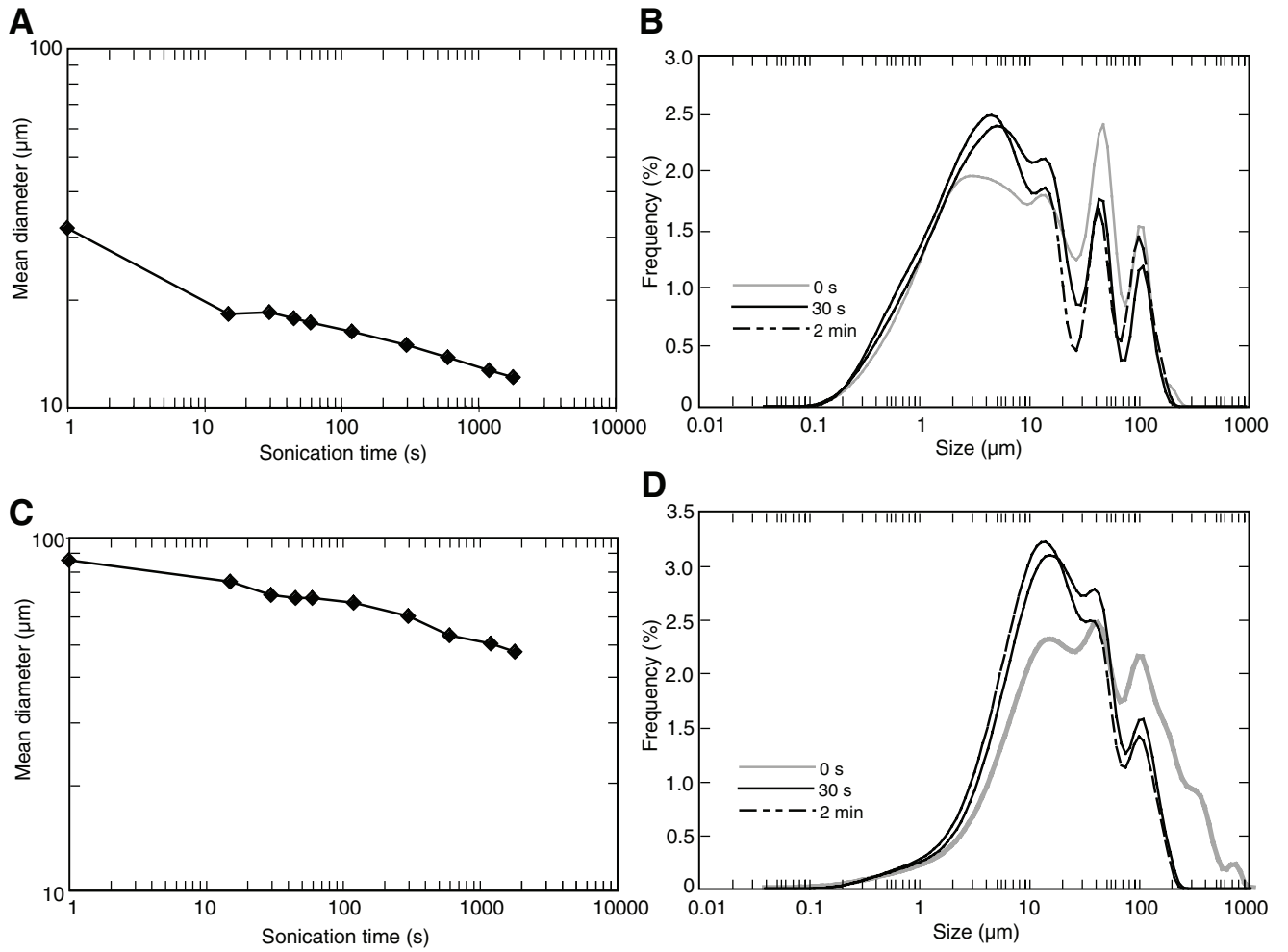
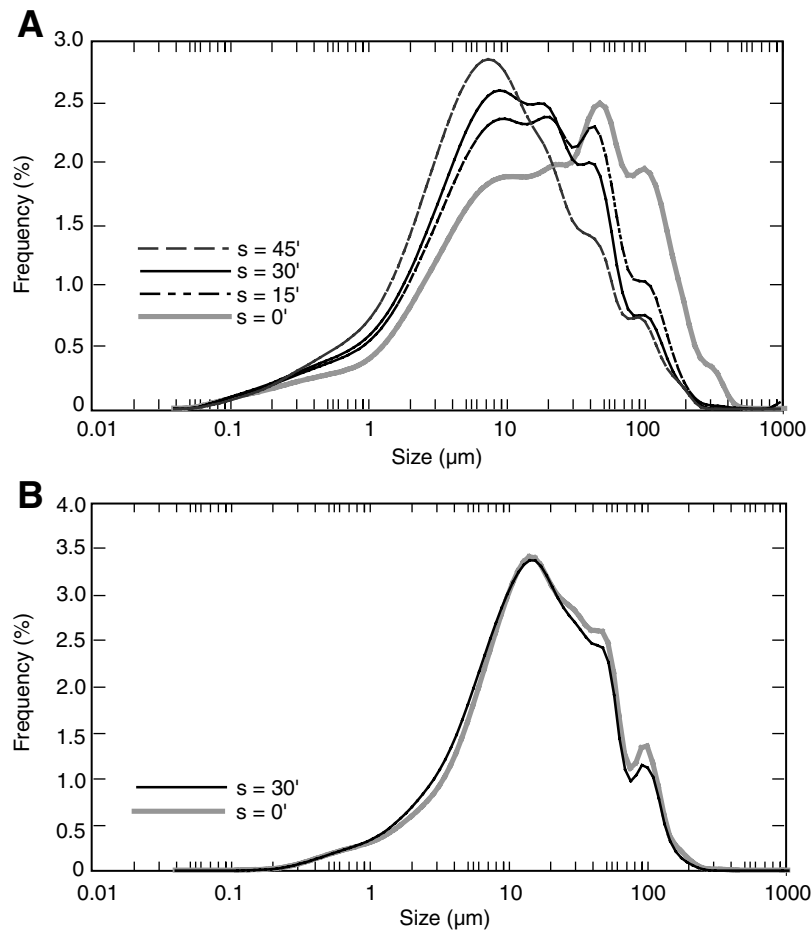**Figure F3.** Site 1225 particle size frequency curve overlays. **A.** Bulk. **B.** Noncarbonate.

Figure F4. Site 1226 particle size frequency curve overlays. **A.** Bulk. **B.** Noncarbonate.
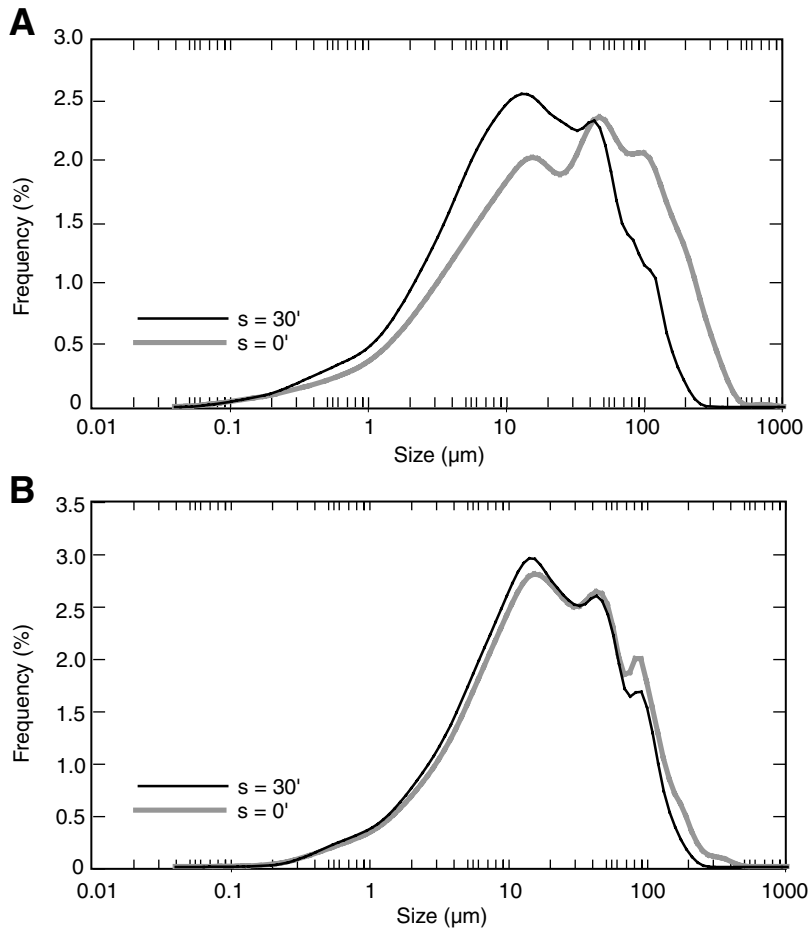
Figure F5. Grain size distributions of representative samples of the main lithologies of Sites 1225 and 1226. **A.** Sample 201-1226E-1H-1, 1 cm. **B.** Sample 201-1226B-6H-3, 0 cm. **C.** Sample 201-1225A-16H-3, 0 cm. **D.** Sample 201-1225A-24H-3, 0 cm. **E.** Sample 201-1226B-47X-2, 13 cm. See the "Appendix," p. 13, for sample depth and statistics. Noncarb = noncarbonate.
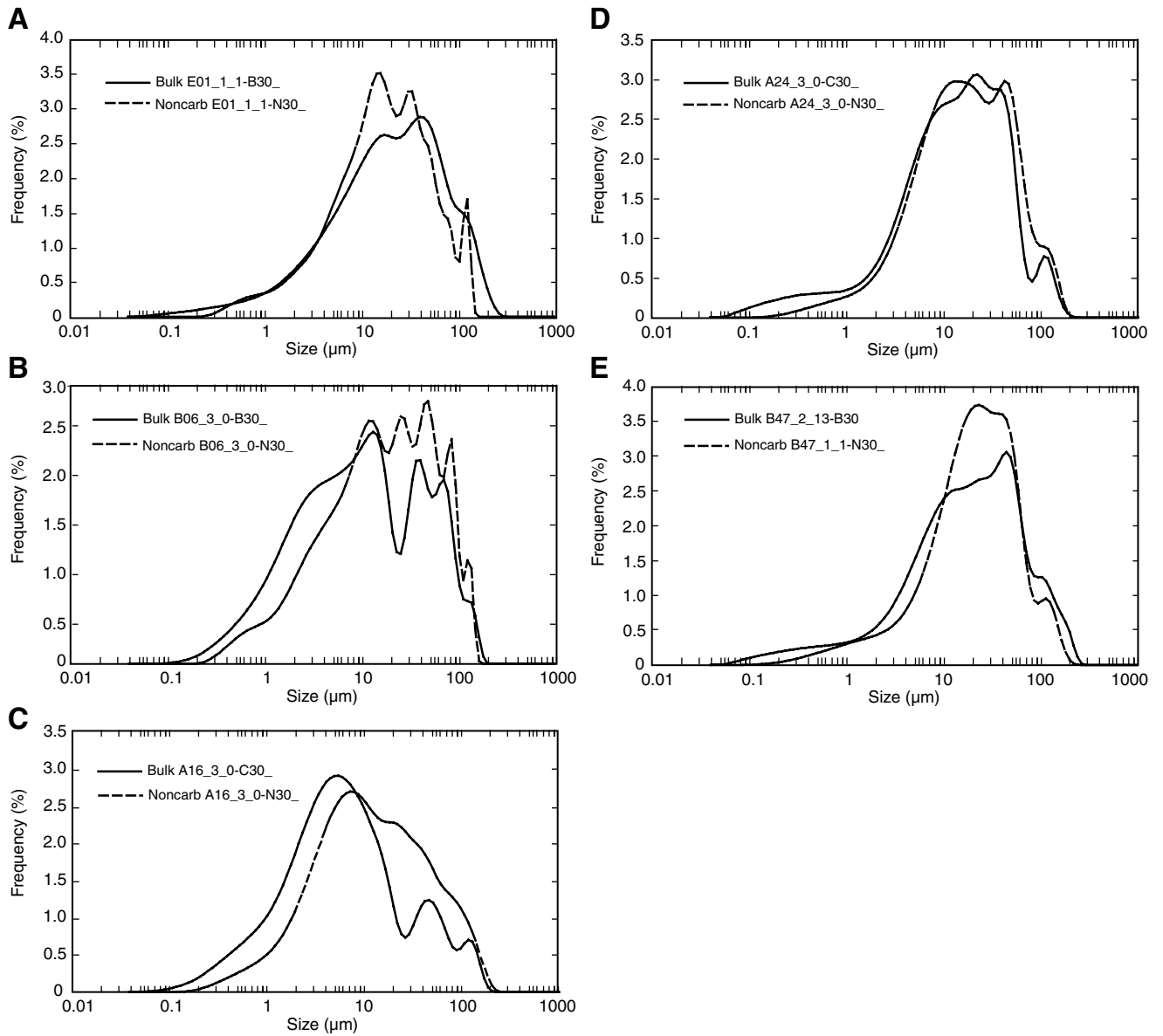
Figure F6. Microtextures of samples from Sites 1225 and 1226. See text for further explanations. **A, B.** Pleistocene nannofossil-rich diatom ooze (Sample 201-1226E-1H-1, 1 cm). **C.** Pleistocene nannofossil-rich mixed radiolarian and diatom ooze (Sample 201-1226B-6H-3, 0 cm). **D.** Pliocene diatom-rich nannofossil-ooze (Sample 201-1225A-16H-3, 0 cm) (cross-polarized light). **E, F.** Late Miocene diatom ooze (Sample 201-1225A-24H-3, 0 cm). (Continued on next page.)
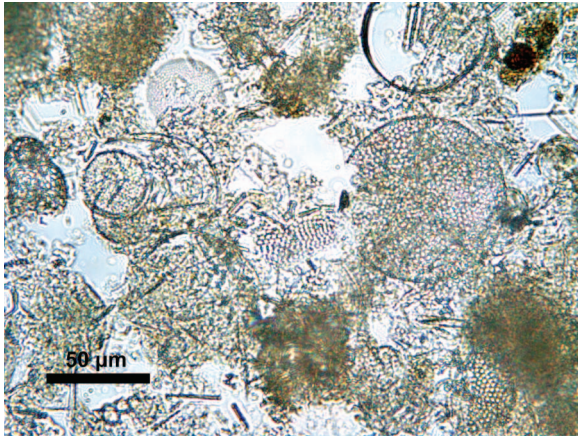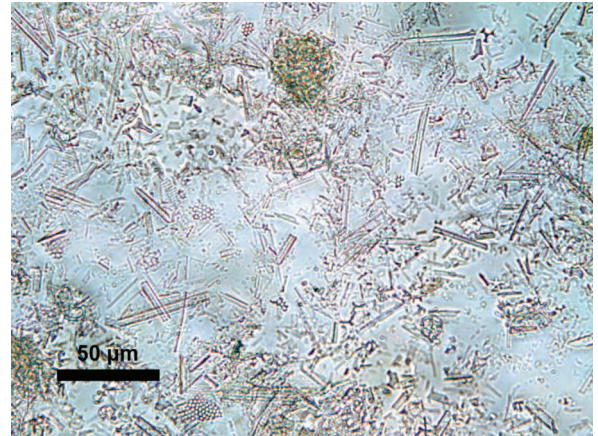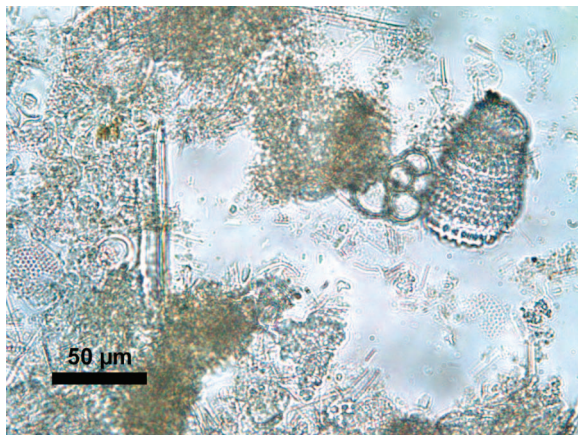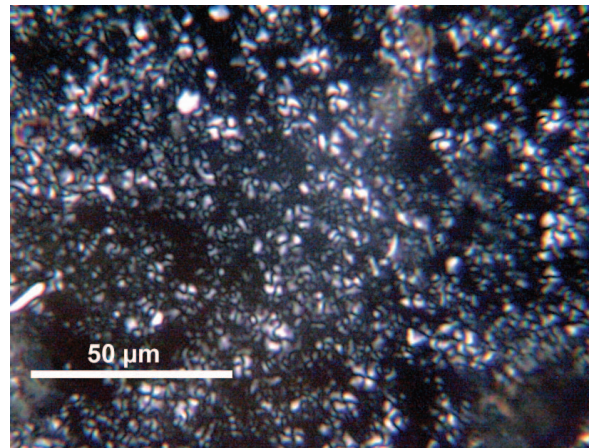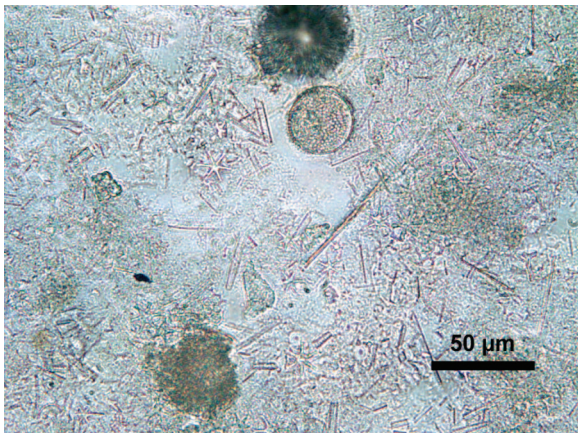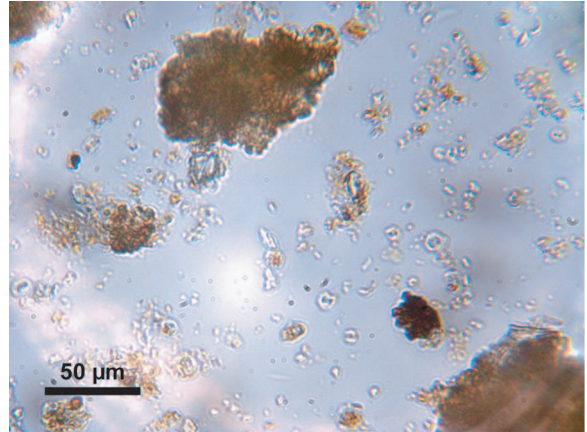
Figure F6 (continued). G. Late Miocene diatom ooze (Sample 201-1226B-31H-3, 19 cm). **H.** Middle Miocene Fe- and Mn-oxide-rich nannofossil ooze (Sample 201-1226B-47X-2, 13 cm). **I.** Sample 201-1226B-47X-2, 13 cm (cross-polarized light).
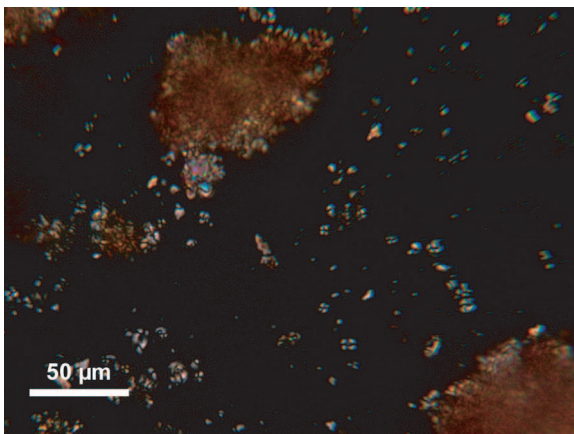
G

H

I

Figure F7. Mean diameter and mode of bulk and noncarbonate fractions after 30 s of sonication time, Site 1225 (D'Hondt, Jørgensen, Miller, et al., 2003).
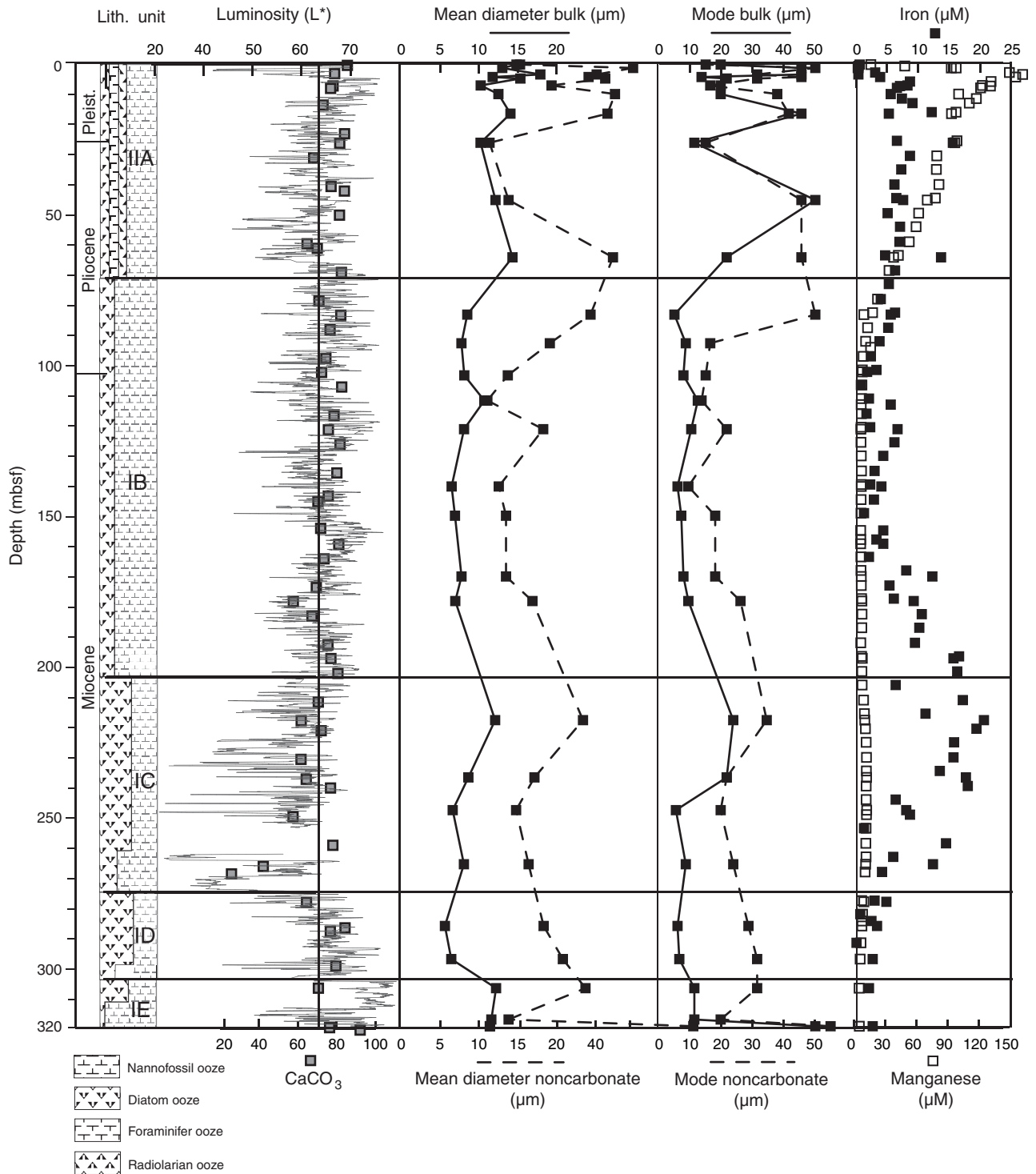
Figure F8. Mean diameter and mode of bulk and noncarbonate fractions after 30 s of sonication time, Site 1226.
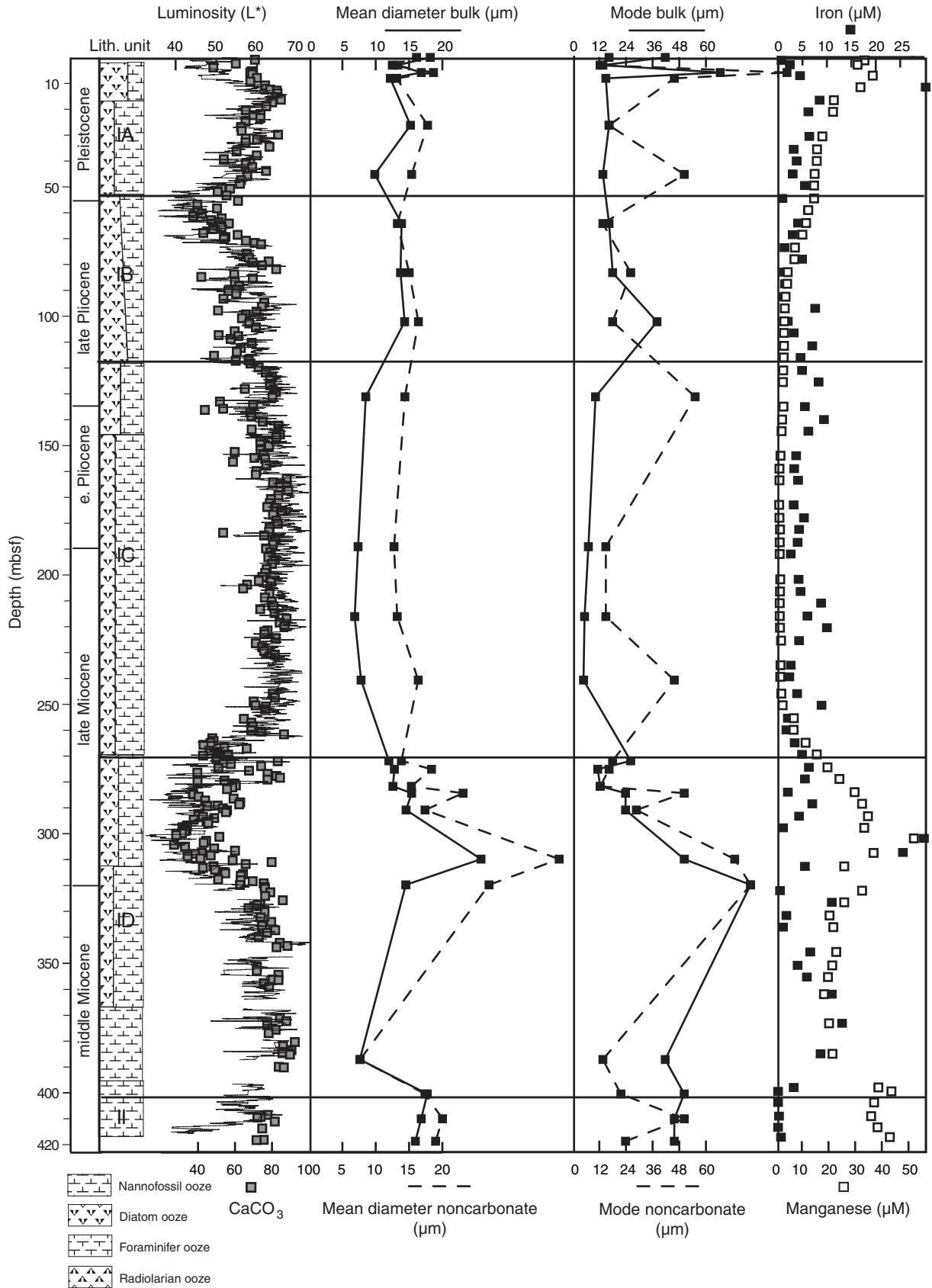
Table T1. Summary of grain size statistics, Site 1225.

Sediment fraction	Sonication (s)/ samples (N)	Mean (µm)	Mode (µm)	Standard deviation	Percentile (µm)				
					d10	d25	d50	d75	d90
Bulk	00/28	18.06	50.22	5.137	2.11	6.278	21.82	62.88	128.7
	15/28	11.4	19.76	4.577	1.531	4.549	12.92	35.79	70.83
	30/28	9.876	9.37	4.424	1.402	4.138	10.96	28.46	58.16
	45/7	8.051	7.775	4.19	1.263	3.396	8.339	21.22	51.01
Noncarbonate	00/20	16.52	14.94	3.274	3.593	8.294	17.55	38.64	70.06
	30/20	14.95	14.94	3.277	3.165	7.381	16	34.96	63.28

Table T2. Summary of grain size statistics, Site 1226.

Sediment fraction	Sonication (s)/ samples (N)	Mean (µm)	Mode (µm)	Standard deviation	Percentile (µm)				
					d10	d25	d50	d75	d90
Bulk	00/28	23.03	50.22	4.982	2.669	8.139	27.36	79.58	161.9
	30/28	13.1	13.61	4.206	1.959	5.403	14.65	38.75	76.82
Noncarbonate	00/28	18.85	39.41	3.61	3.253	8.204	20.35	50.47	98.23
	30/28	16.15	33.92	3.47	2.913	7.253	17.52	42.62	80.77